

**Gamma Ray Observations of Cygnus X-1 with the  
Oriented Scintillation Spectrometer Experiment**

B. F. Phlips<sup>1</sup>, G. V. Jung<sup>1</sup>

Universities Space Research Association, Washington DC, 20024

M. D. Leising

Department of Physics and Astronomy, Clemson University, Clemson, SC 29634

J. E. Grove, W. N. Johnson, R. L. Kinzer, R. A. Kroeger, J. D. Kurfess, M. S. Strickman

Naval Research Laboratory, Code 7650, Washington DC, 20375

D. A. Grabelsky, S. M. Matz, W. R. Purcell, and M. P. Ulmer

Department of Physics and Astronomy, Northwestern University, Evanston, IL 60208

K. McNaron-Brown<sup>1</sup>

Institute for Computational Sciences and Informatics, George Mason University, Fairfax,

VA 22030

<sup>1</sup> Postal address: Code 7650, Naval Research Laboratory, Washington DC, 20375

## **Abstract**

We report on ~120 days of observations of Cygnus X-1 with OSSE onboard the Compton Observatory. Emission is detected in the range 50 keV to 1 MeV and we find evidence for a continuum of hard X-ray flux levels rather than the existence of distinct flux states. Comparisons of the source spectra with various theoretical models show that an exponentially truncated power law best describes the average spectrum in the OSSE energy band. Although we have measured a new minimum in the hard X-ray flux from the source, no evidence was found for either a broad 1 MeV feature or a narrow 511 keV line previously reported in association with a low flux state. Upper limits on such emission features are an order of magnitude lower than earlier reported detections. The 5.6-day periodicity of the source measured at optical wavelengths was not detected with a sensitivity to the rms modulation fraction of 5% in the 60-140 keV energy band.

**Subject:** Gamma Rays: Observations-Black Holes-stars:individual (Cyg X-1)-  
X-Rays:Binaries

## 1 INTRODUCTION

Cyg X-1, one of the brightest and most extensively studied gamma ray sources in the sky, is a 5.6-day binary system consisting of a blue supergiant and a compact companion of mass  $\sim 6.3 M_{\odot}$  (Gies et al. 1986, Dolan et al. 1992). If the compact object has a mass greater than  $3 M_{\odot}$ , Cyg X-1 is generally considered a prime black hole candidate, and it has become the prototype for black hole characterization and modeling. The possible presence of features in the spectrum of Cyg X-1 has been suggested as a useful criterion for distinguishing black hole systems from those containing neutron stars (Liang et al. 1992). In particular, features such as soft X-ray excesses or gamma-ray bumps in the hard X-ray/gamma-ray energy band have been proposed as signatures of black holes, giving special importance to an improved knowledge of the detailed shape of the Cyg X-1 spectrum at high energies.

The high-energy radiation from Cyg X-1 is thought to be emission from an accretion disk surrounding a black hole (Shapiro, Lightman & Eardly 1976). The soft 1-10 keV X-ray spectrum has traditionally been described by a dominant “low” state with occasional periods of “high” state emission (e.g., Friedhorsky, Terrell and Holt 1983). The hard X-ray flux is well represented by a thermal Comptonization spectrum (Sunyaev and Titarchuk 1980; Ling et al. 1983). Using HEAO-3 data, Ling et al. (1987) identified three distinct levels for the 45-140 keV flux occurring during the low X-ray state, which they labeled  $\gamma_1$ ,  $\gamma_2$  and  $\gamma_3$ , with  $\gamma_1$  being the state with the lowest 45-140 keV flux. The intensity of the hard X-ray flux may be anti-correlated with the intensity of the soft X-ray flux (Bassani et al. 1989). A gamma-ray excess, characterized by a 1.2 MeV wide gaussian at 1 MeV with a line flux of  $1.6 \times 10^{-2}$  photons  $\text{cm}^{-2} \text{s}^{-1}$ , was detected in fall 1979 when Cyg X-1 was in the  $\gamma_1$  state (Ling et al. 1987). A weak  $2\sigma$  detection of a narrow 511 peak was later reported from analysis of the HEAO data during the same episode (Ling et al. 1989). Other groups have also reported measurements of MeV emission from Cyg X-1 (see Owens and McConnell. 1992 for a review of the MeV observations, including calculations of equivalent line flux intensities). For example, Baker et al. (1973) described a spectral feature near 2 MeV, with positive emission up to 6 MeV. Mandrou et al. (1978) observed fluxes up to 3 MeV, although they did not see any bumps. McConnell et al. (1989) reported detecting a hard spectral component out to 9 MeV. A general review of Cyg X-1 studies was written by Liang and Nolan (1984).

Although there is a wide spread of energies over which MeV emissions have been reported, these measurements suggest periods of spectral hardening in the MeV region beyond a simple extrapolation from the hard X-ray spectrum. There are, however, a considerable number of experiments (Schoenfelder et al. 1974; White et al. 1980; Nolan 1982; Varendorff et al. 1990) reporting featureless hard X-ray and gamma-ray spectra, and the limits derived from these experiments are well below the flux values measured by other experiments. In addition, Harris et al. (1993) derived upper limits for flaring episodes of 12 or more days from the long-term data base of the gamma-ray spectrometer on SMM, and McConnell et al. (1994) recently reported no evidence for MeV features from Cyg X-1 in data from the COMPTEL experiment on the Compton Observatory.

The presence of enhanced emission near 1 MeV, such as detected with HEAO-3, was interpreted by Liang and Dermer (1988) as the emergent radiation from a photon-starved pair-dominated thermal plasma. In this picture, the hard X rays are produced by thermal Comptonization of a copious soft photon source farther out in the disk, in accord with earlier models of the hard X-ray spectrum of Cyg X-1 and the innermost region, shielded from the soft photon flux, reached MeV temperatures. Spectral complexity is also found in the X-ray regime. Done et al. (1992) demonstrated the presence of a reflection component in EXOSAT and HEAO-1 observations, and argued that a multi-temperature thermal Comptonization model was required to give a good fit to the Cyg X-1 spectrum. Recently, Haardt et al. (1993) suggested that thermal Comptonization in an accretion-disk corona is simply described by a power law with an exponential cutoff. Zdziarski et al. (1994) combined optically thin Comptonization and reflection into a model consisting of an exponentially cutoff power law with reflection in a form useful for data analysis. The excellent sensitivity of the OSSE measurements provide spectra with adequate precision to test these theoretical models.

In this paper, we present results of measurements of Cygnus X-1 using the Oriented Scintillation Spectrometer Experiment (OSSE) on the Compton Gamma Ray Observatory (CGRO). Given the importance of testing the models of the source and resolving the conflicting nature of some of the previous measurements, OSSE devoted 122 days to observing the source at different intensity levels during the first four years of the CGRO mission. The shape of the spectrum, the search for narrow and broad spectral features, the light curve of daily flux averages, the flux levels of the source, and correlations of hardness ratios are addressed. We describe OSSE observations of Cyg X-1 in Section 2, the temporal variability analysis in Section 3, and spectral analysis in Section 4. Our

search for spectral features is presented in Section 5, and discussion of the results is given in Section 6.

## 2 OBSERVATIONS

The Oriented Scintillation Spectrometer Experiment is one of four instruments on the Compton Gamma Ray Observatory. The observatory was launched on board the space shuttle Atlantis on 5 April 1991 and has been operating in a 28 degree inclination low earth orbit. OSSE consists of four identical and independently moveable NaI-CsI phoswich detectors sensitive to gamma rays between 50 keV and 10 MeV. Each detector has a tungsten collimator which defines a  $3.8^\circ \times 11.4^\circ$  FWHM rectangular field of view, and active shielding provided by NaI anticoincidence detectors configured in an annulus around the main detector. Each detector has an effective area of  $\sim 500 \text{ cm}^2$  at 511 keV. Eight- or sixteen-second spectra are accumulated on board and then transmitted to Earth for spectroscopic analysis, while limited event-by-event or fast rate samples over certain energy bands are also accumulated in parallel for timing analysis. We will report here on analysis of the spectroscopy data. Timing analysis of these data at mHz to kHz frequencies is not considered here and will be presented elsewhere (see Bridgman et al. 1994 for an early analysis). Spectra are integrated into two minute intervals, alternately viewing the source field and background fields offset by  $\sim 5$  degrees. Using the known response of the detectors, the background-subtracted count spectra are converted into photon spectra using a forward-folding technique. A full description of the instrument and standard methods of data analysis are given by Johnson et al. (1993).

OSSE observed Cyg X-1 during 17 intervals, each spanning one or more days in the first four years of the CGRO mission, for a total of  $\sim 2.4 \times 10^6$  live seconds of background-subtracted spectroscopy data. Table 1 summarizes these observations. The large spread in total live times of the different observations resulted from variations in the number of detectors used in the observation (1 to 4) and the length and quality of each observation. These data are not a random sample of the flux levels of the source because four of the observations, numbers 6, 7, 8 and 10, were in response to a low hard X-ray state detected by the Burst and Transient Source Experiment (BATSE) on CGRO (Fishman et al. 1989). The observations were analyzed for each detector and each day separately, and the spectra were added at the end of the analysis.

### 3 TEMPORAL ANALYSIS

The integrated flux in the 45-140 keV band for each day of data is shown in Figure 1, where the x-axis represents days of data with a short break between viewing periods that is not representative of the actual time between the observations. The energy band was chosen to match the band used in the analysis of the HEAO-3 data. The data between 60 and 140 keV were fit with a thermal bremsstrahlung spectrum and the resulting fit was used to calculate a 45-140 keV flux. For the days where the instrument configuration provided spectra down to 40 keV, the calculated and measured flux were in agreement.

As seen in Figure 1, there are no obvious discrete states, but rather a continuum of intensities. This becomes clearer when the daily flux is observed over a long period of time, as is done by the BATSE experiment (Paciesas et al. 1994). Compared with the historic  $\gamma_1$ ,  $\gamma_2$  and  $\gamma_3$  levels, the observations of February 1994 (CGRO viewing period 318) revealed a flux intensity of  $\sim 1/5$  the previously reported lowest flux in this band. The source has therefore a greater range of intensities than previously measured. Note, however, that no OSSE measurements have been performed at intensities comparable to the  $\gamma_3$  level.

The light curve shown in Figure 1 can be searched for periodicities, in particular for the 5.6-day orbital periodicity. The data set is sparse, with only  $\sim 100$  days of data out of a 1024 day interval, with the contiguous daily data sets varying from two days to two weeks in length. The measurements are therefore not very sensitive to periodicities between a few weeks and a few months. For this analysis the data were binned into individual days; therefore the shortest detectable variability is two days. We calculated the Fast Fourier Transform of the mean subtracted data set for the first 1024 days of the mission and found most power at low frequencies due to overall trends in the data; more specifically, the significant drop in flux in February 1994. To detrend the data, we subtracted a fifth order polynomial in time and calculated the Fast Fourier Transform of the residuals. We find no evidence for periodicity in this sparse data set, other than a peak at very low frequency due to the data sampling. The upper limit to the amplitude of a 5.6-day periodicity is  $5 \times 10^{-3}$  photons  $\text{cm}^{-2} \text{s}^{-1}$  in the 60-140 keV band, corresponding to an rms modulation fraction of less than 5%.

### 4 SPECTRAL ANALYSIS

The spectrum for the sum of all data through May 1995 is shown in Figure 2. The spectrum is smooth, without breaks or line features. It extends from 60 keV, the lower threshold used in this spectral analysis, to  $\sim 1$  MeV, where the flux level falls below the OSSE sensitivity. The high statistical precision of the Cyg X-1 spectrum permits differentiation among theoretical models to much higher energies than previously possible. We use the four different functional forms to fit the data. The first is a simple two-parameter thermal bremsstrahlung model described by

$$\Phi(E) = KE^{-1}e^{(-E/kT)}, \quad (1)$$

where  $\Phi(E)$  is the flux at energy  $E$ ,  $K$  is the normalizing constant and  $T$  is the temperature. The second functional form we use is the three-parameter thermal Comptonization spectrum of Sunyaev and Titarchuk (1980). It is derived for a spherical, uniform electron plasma with Thomson depth  $\tau = n_e\sigma_T R$ , where  $n_e$  is the electron density and  $R$  is the radius of the region, and is strictly valid in the nonrelativistic ( $kT \ll m_e c^2$ ), diffusive ( $\tau \gg 1$ ) regime. Higher temperature corrections have been derived by Titarchuk (1994), and Hua and Titarchuk (1995), but Monte Carlo simulations including pair production (Skibo et al. 1995) are required to provide accurate representations at all temperatures and optical depths. However, the Monte Carlo results and the refined model of Titarchuk (1994) agree closely with the original model of Sunyaev and Titarchuk (1980) for the parameter values of Cyg X-1.

The third functional form employed is a three-parameter exponentially truncated power law given by

$$\Phi(E) = KE^{-\Gamma}e^{(-E/E_c)}, \quad (2)$$

where  $\Gamma$  is the photon spectral index and  $E_c$  is the cutoff energy. We also include the possibility that some fraction of the emission described by equation (2) is incident on a cold optically thick scattering medium for the fourth functional form we employ. The effects of Compton reflection are contained in a code provided by Zdziarski (1995a). The model contains a reflection parameter that is proportional to the solid angle covered by the reflection medium: a reflection coefficient of 1 is a source just above an infinite plane of reflecting material, a coefficient of two implies that the sources is embedded in the reflecting medium.

Table 2 lists the fits of these various models to the sum of all the Cyg X-1 data. The normalizing energy was fixed at 100 keV and all daily fits were over the energy range from 60 keV to 4 MeV. When all the observations are added together, the systematic differences among detectors become important and the spectra have to be fit detector by detector with the various models. The difference between the variance in the distribution of the parameters obtained and the square of the error in the fit parameters is used as a measure of systematic errors. The statistical errors are 68% confidence intervals. The parameters in Table 2 are listed as the average of that parameter for all detectors with the fit error followed by the systematic error, in parentheses. The reduced  $\chi^2$  quoted is the average  $\chi^2$  per degree of freedom of the fits over the detectors. The best fit models given by the functional form of equation (2) and a thermal Comptonization model are overlaid on the data in Figure 2.

The model with an exponentially truncated power law gives the best fit to the data. The thermal bremsstrahlung and the thermal Comptonization models both diverge from the measured spectrum at higher energies where they underestimate the flux from the source. The exponentially truncated power law with reflection produces a fit to the data slightly worse than without reflection, and the fit improves as the amount of reflection decreases. The difference in the photon spectra between the model with and without reflection occurs mostly at the lower end of the OSSE energy range, where the systematic errors in the instrument efficiency and calibration are largest. The confidence in rejecting models based solely on the lowest energy bins is therefore smaller than the confidence in rejecting models which diverge at higher energies like the thermal bremsstrahlung and thermal Comptonization models. The exponentially truncated power law is also the best model when each observation is summed and fitted separately. Table 3 lists the results of the fits to each observation, along with the source luminosity in the 60 keV-1 MeV range, assuming a Cyg X-1 distance of 2.5 kpc. The statistical error in the luminosity is 1% or better for all observations.

The optically thin thermal bremsstrahlung model still provides a good fit to the daily spectra. This simple two-parameter model is used to study the temperature-intensity dependence of the source. Figure 3 shows that the temperature of the source and the intensity vary within a limited range, except for a few excursions to the low temperature-low amplitude regime. During the very low flux observation of February 1994, the temperature of the source was  $\sim 70$  keV compared with 110 keV for the other observations. Note that the scatter in the points on this figure and the following figures is

much larger than the statistical or systematic errors. Alternatively fitting the daily data with the thermal Comptonization model derived by Sunyaev and Titarchuk (1980), we find a similar scatter in the optical depth parameter, with the temperature fairly constant with a mean of 65 keV and a standard deviation of less than 5 keV. With the temperature fixed at 65 keV, the optical depth-intensity distribution is as shown in Figure 4.

In Figure 5, we display spectra in terms of  $E^2\Phi(E)$  in order to highlight the energy of peak power output in the OSSE band and emphasize the differences between spectra measured at different flux states. The spectrum with open squares is the sum of all days with a flux (in the 45-140 keV band) of less than  $0.06 \text{ photons cm}^{-2} \text{ s}^{-1}$ . The spectra with filled squares, open circles and filled circles are for a flux between 0.06 and 0.08, between 0.08 and 0.105 and greater than 0.105  $\text{photons cm}^{-2} \text{ s}^{-1}$ , respectively. The low amplitude spectra are more like a power law than the other data. If a power law is assumed for the observation with the lowest amplitude spectrum, observation 10, the best fit is for an amplitude of  $7.5 \pm 0.1 \times 10^{-2} \text{ photons cm}^{-2} \text{ s}^{-1} \text{ MeV}^{-1}$  at 100 keV and a power law index of  $-2.72 \pm 0.03$  with a  $\chi^2$  probability of 0.3.

## 5 SEARCH FOR LINE FEATURES

To search for any spectral features associated with specific flux levels that would have been averaged out in the total spectrum, the data were divided into individual days and each day was analyzed separately. Following the analysis of Ling et al. (1987), we searched for the presence of MeV bumps by fitting each day of data with a thermal bremsstrahlung spectrum and a 1.2 MeV wide gaussian line feature centered at 1 MeV. Near the  $\gamma_1$  flux level, an increase in the fit 1 MeV amplitude would be expected. The fit amplitudes are shown in Figure 6a. We see no significant amplitude for a broad gaussian feature for any flux level of the source. When all the data are added together, as in Figure 2, the 90% confidence level (CL) upper limit to the 1 MeV line is  $4 \times 10^{-4} \text{ photons cm}^{-2} \text{ s}^{-1}$ , compared to the flux of  $1.6 \times 10^{-2} \text{ photons cm}^{-2} \text{ s}^{-1}$  measured by Ling et al. The 95% CL upper limit for a 1-1.5 MeV wide feature near 4 MeV is  $2.0 \times 10^{-5} \text{ photons cm}^{-2} \text{ s}^{-1}$ .

The search for lines can be repeated at any energy and width. Given the previous reports of a narrow 511 keV line, we fit the data for a narrow ( $<$  instrument resolution) 511 keV line for each day of data. These results are shown in Figure 6b. We do not find any days with a significant excess 511 keV emission nor a correlation between the 511 keV emission and the overall source strength. The 90% CL upper limits to the amplitude are

between  $0.5$  and  $1.0 \times 10^{-3}$  photons  $\text{cm}^{-2} \text{s}^{-1}$  for most days. The 90% CL upper limit for a narrow 511 keV in the total spectrum is  $7 \times 10^{-5}$  photons  $\text{cm}^{-2} \text{s}^{-1}$ .

Since Ramaty et al. (1981) predict a broad 511 keV feature (FWHM  $\sim 160$  keV), we also searched for a 160 keV wide peak at 511 keV. The results show no significant positive detections. The fit flux values for the broad line are significantly larger than for the narrow line because the broad line has a larger effect on the underlying continuum spectrum represented by a thermal bremsstrahlung model. Still, the derived flux values provide new limits to theoretical models with a 90% CL upper limit of 1 to  $3 \times 10^{-3}$  photons  $\text{cm}^{-2} \text{s}^{-1}$  for most days. The 90% CL upper limit for a broad 511 keV feature in the total spectrum is  $2 \times 10^{-4}$  photons  $\text{cm}^{-2} \text{s}^{-1}$ .

## 6 DISCUSSION

The variability of Cyg X-1 at gamma ray energies, as seen Figure 1, is a factor of  $\sim 15$ , much greater even than the factor of  $\sim 3$  measured during the HEAO-3 mission. However, the variability does not seem to be between discrete states but rather among a continuous range of possible flux values. The optically thin thermal bremsstrahlung fits to the individual days of data show that the source usually fluctuates in a seemingly random fashion in a narrow range of intensity-temperature phase-space. This is unlike the behaviour observed in GRO J0422+32, where the temperature is monotonically increasing in time as the transient decreases in brightness (Kroeger et al., 1995).

The spectrum is best described by a model with optically thin Comptonization. However, a preliminary analysis reveals that this model cannot be applied to contemporaneous GINGA (Ebisawa, 1994) and OSSE data. A more complex model using an exponentially truncated power law with an angle dependent reflection component might fit both sets of data simultaneously (Zdziarski et al., 1995b). Using the exponentially truncated power law model to find the maximum in the luminosity per decade and correlating that with the luminosity in the 60 keV-1 MeV band, the relationship shown in Figure 7 is obtained. The maximum in the distribution of luminosity per decade seems correlated to the total luminosity. The spectrum for the lowest intensity observation, observation 10, is then interpreted as the same model with a maximum at  $\ll 60$  keV in the distribution of luminosity per decade, instead of the more typical 100 keV, causing the power law-like appearance of this spectrum.

Extrapolating the exponentially truncated power-law model to lower energies, we find that the calculated flux in the 3-11 keV range for observation 10 (the lowest intensity observation in the OSSE energy band) is  $\sim 3$  times larger than for observation 1, a typical observation. This anticorrelation between the extrapolated low energy X-ray flux and the measured gamma ray flux is consistent with earlier observations (Priedhorsky et al. 1983) and is not very model dependent. The crossover energy for the low intensity gamma ray spectra to become dominant is between 10-20 keV, depending on which spectra are compared.

We have searched for the amplitude of a broad MeV bump, a narrow 511 keV line, and of a broad 511 keV line. The distribution of fit MeV amplitudes (Figure 8) is gaussian, with a small non-zero mean, indicating the underlying thermal bremsstrahlung distribution under-estimates the continuum flux at 1 MeV by  $\sim 5 \times 10^{-4}$  photons  $\text{cm}^{-2} \text{s}^{-1}$ . There is no evidence for an excess of points at high flux values, and no single day with an amplitude near that measured by Ling et al. (1987) over a 12 day period. The width of the distribution in Figure 8 is consistent with the uncertainty in the amplitudes histogrammed. Since no strong signal was found, upper limits are derived for such features. These upper limits are lower than previous measurements and constrain the models for Cyg X-1. The 90% confidence level upper limit to the 1 MeV bump flux is in the  $1-4 \times 10^{-3}$  photons  $\text{cm}^{-2} \text{s}^{-1}$  range for most days. This clearly demonstrates that the MeV bump is not systematically associated with the  $\gamma_1$  state. If MeV bumps of the intensity reported by Ling et al. do exist, they must be transient within the  $\gamma_1$  state. Our non-detection of MeV features limits the duty cycle of such a process. For 1-day emission episodes, there is a 90% probability we would have detected a duty cycle greater than 2.3%, or more than 25 outbursts over the first three years of the mission. For 4-day episodes the duty cycle must be less than 4.5%, and for 14-day episodes, the duty cycle must be less than 9%, which corresponds to  $\sim 6.5$  outbursts over the mission so far. Harris et al. (1994) obtained a 95% upper limit of 4.1% on the duty cycle for 12-day episodes.

According to the models of Dermer et al. (1989) and the compilation of data by Bassani et al. (1989), there should be an anticorrelation between the hard X-ray flux and the gamma ray flux. We have binned our data in two bands, 0.06-0.4 MeV and 0.4-1.5 MeV and plotted the high energy band versus the low energy band, for a direct comparison with Bassani et al. (Figure 9). From the total data set, one would conclude that there is a correlation, not an anticorrelation, between the gamma ray flux and the hard X-ray flux. This is consistent with our earlier interpretation of higher temperatures at higher flux. The

anticorrelation modeled by Dermer and Liang was for a fixed accretion rate. However, it is likely that the changes measured are due to a change in accretion rate. In that case, the predicted hard X-ray and gamma ray components would rise and fall together and would be correlated, as observed. The correlation coefficient for these data, when weighed by and including only the error in the high energy flux, is 0.72, corresponding to a probability that the variables are not correlated of  $< 0.01$ . If only data with hard X-ray flux  $> 0.20$  photons  $\text{cm}^{-2} \text{s}^{-1}$  are considered, the correlation coefficient of this ratio is 0.03, implying no correlation between the fluxes during most observations.

The 0.4 -1.5 MeV band is not optimized for daily OSSE observations of Cyg X-1, since the source is not detected beyond  $\sim 800$  keV on a daily basis. This energy band was selected to provide a direct comparison with the analysis of Bassani et al. To better check our compatibility with the model of Dermer et al. that postulates a pivot point near 100 keV, we have derived the hardness ratio between the 200-400 keV band and the 60-80 keV band. A spectral shape independent of amplitude would produce a horizontal line in this plot, and the expected anticorrelation would be seen as a decreasing curve. From Figure 10, we see the same pattern as in the temperature-amplitude scatter plots. There is a positive correlation (correlation coefficient of 0.32) between the hardness ratio and the 60-80 keV flux for the low amplitude points only ( $< 0.7$  photons  $\text{cm}^{-2} \text{s}^{-1}$  in the 60-80 keV band), again consistent with higher temperatures at higher flux. But for the dense, high hardness ratio cluster of data ( $> 0.7$  photons  $\text{cm}^{-2} \text{s}^{-1}$  in the 60-80 keV band and  $> 0.035$  photons  $\text{cm}^{-2} \text{s}^{-1}$  in the hardness ratio), there is an anticorrelation (correlation coefficient of -0.48) between the ratio and the low energy flux.

We hope to shed further light on this correlation-anticorrelation pattern by acquiring more data on Cyg X-1 when it is at intermediate or very bright flux levels.

## **Acknowledgments**

We would like to thank Dr. C. D. Dermer for his helpful comments during the writing of this paper. This work was supported by NASA grant DPR S-10987C.

## References

- Baker, R.E. et al. 1973, *Nature Phys. Sci.*, 245, 18
- Bassani, L., Dean, A. J., Di Cocco, G., Pirotti, F., and Stephen, J.B. 1989, *Astrophys. J.*, 343, 313
- Bridgman, W.T. et al. 1994, *Second Compton Symposium*, AIP Conf. Proc 304, 225
- Dermer, C.D., and Liang, E. P. 1989, AIP Conf. Proc. No. 170, ed. N. Gehrels (AIP, NY), 326
- Done, C., Mulchaey, J. S., Mushotsky, R. F., and Arnaud, K. A. 1992, *Astrophys. J.*, 395, 275
- Dolan, J.F., and Tapias, S. 1989, *Astrophys. J.*, 344, 830
- Ebisawa, K. 1994, private communication
- Fishman, G.J. et al. 1989, *Proc. of the Gamma Ray Observatory Workshop*, Goddard Space Flight Center, Greenbelt, MD, ed. W. N. Johnson, 2
- Gies, D.R., and Bolton, C. T. 1986, *Astrophys. J.* 304, 371
- Haardt, F., and Maraschi, L. 1993, *Astrophys. J.*, 413, 507
- Harris, M.J., Share, G. H., Leising, M. D., and Grove, J. E. 1993, *Astrophys. J.*, 416, 601
- Harris, M.J., Share, G. H., and Leising, M. D. 1994, *Second Compton Symposium*, AIP Conf. Proc 304, 250
- Johnson, W.N. et al. 1993, *Astrophys. J. Supp.*, 86, 693
- Kroeger, R.A. et al. 1995, submitted.
- Liang, E. P., and Nolan, P. 1984, *Space Sci. Rev.*, 38, 353
- Liang, E. P., and Dermer, C. D. 1988, *Astrophys. J.*, 325, L39
- Liang, E.P. et al. 1992, *Compton Observatory Science Workshop*, ed. C.R. Shrader, NASA Conf. Pub. 3137, 174
- Ling, J.C., Mahoney, W. A., Wheaton, W. A., Jacobsen, A. S., and Kaluzienski, L. 1987, *Astrophys. J.*, 321, L117
- Ling, J.C., and Mahoney, W. A. 1989, *Astrophys. J.*, 343, 157
- Mandrou, P., Niel, M., Vedrenne, G., Dupont, A., and Hurley, K. 1978, *Astrophys. J.*, 219, 288
- McConnell, M.L., Forrest, D. J., Owens, A., Dunphy, P. P., Vestrand, W. T., and Chupp, E. L. 1989, *Astrophys. J.*, 343, 317
- McConnell, M.L. et al. 1994, *Astrophys. J.*, 424, 933
- Owens, A., and McConnell, M. L. 1992, *Comments Astrophys.*, 16, 205
- Nolan, P.L., 1982, PhD thesis, UCSD

- Paciesas, W.S. et al. 1994, Proc. NATO Advanced Study Institute Conf., Les Houches, ed.  
M. Signore (Kluwer, The Netherlands)
- Priedhorsky, W.C., Terrell, J., and Holt, S. S. 1983, *Astrophys. J.*, 270, 233
- Ramaty, R., and Meszaros, P. 1981, *Astrophys. J.*, 250, 384
- Schonfelder, V., and Lichti, G. 1974, *Astrophys. J.*, 192, L1
- Shapiro, S.L., Lightman, A.P., and Eardly, D.M. 1976, *Astrophys. J.*, 204, 187
- Sunyaev, R.A., and Titarchuk, L. G. 1980, *Astron. Astrophys.*, 86, 121
- Ueda, Y., Ebisawa, K., and Done, C. 1994, *PASJ*, 46, 107
- Varendorff, M., von Ballmoos, P., Graser, U., and Sconfelder, V. 1990,  
Proc. 21st ICRC, 1, 200
- White, R.S., Dayton, B., Gibbons, R., Long, J. L., Zanrosso, E. M., and Zych, A. D.  
1980, *Astrophys. J.*, 284, 608
- White, T.R., Lightman, A. P., and Zdziarski, A. A. 1988, *Astrophys. J.*, 331, 939
- Zdziarski, A.A., Fabian, A. C., Nandra, K., Celotti, A., Rees, M. J., Done, C.,  
Coppi, P. S., and Madejski, G. M. 1994, *Mon. Not. R. Astron. Soc.*, 269, L55
- Zdziarski, A.A. et al. 1995a, private communication
- Zdziarski, A.A. et al. 1995b, in preparation

Table 1: OSSE observations of Cyg X-1.

No.	Dates <sup>(a)</sup>	Viewing Period <sup>(b)</sup>	Total Live Seconds <sup>(c)</sup> x10 <sup>4</sup>
1	91/150-165	2	39.2
2	91/220-227	7.0	10.9
3	91/332-346	15	25.4
4	92/336-357	203	21.8
5	93/040-053	209	20.1
6	93/080-082	212	5.4
7	93/133-134	221	2.5
8	93/151-154	223	7.0
9	93/274-277	303.4	7.9
10	94/032-039	318.1	43.8
11	94/144-145	328	2.7
12	94/158-159	331	2.8
13	94/165-169	331.5	12.1
14	94/174-175	332	1.3
15	94/192-193	333	2.5
16	95/130-143	419.5	9.7
17	95/143-156	420	8.8

(a) dates are year/day of year.

(b) GRO mission timeline viewing period identification.

(c) the total livetime is the sum of the livetimes of the detectors observing the source.

Table 2: Fits of various models to the 122-day summed Cyg X-1 spectrum.

Model	Amp. @ 100 keV ( $\gamma \text{ cm}^{-2} \text{ s}^{-1} \text{ MeV}^{-1}$ )	kT, $E_c$ <sup>(a)</sup> (keV)	Photon Index	$\tau$	$\chi^2/\text{DOF}$
Thermal Bremsstrahlung	$0.476 \pm 0.002 (\pm 0.017)$	$108 \pm 1 (\pm 5)$			50.0
Thermal Comptonization	$0.465 \pm 0.001 (\pm 0.021)$	$65 \pm 1 (\pm 3)$		$1.94 \pm 0.04 (\pm 0.05)$	19.6
Power law times exponential	$0.470 \pm 0.001 (\pm 0.017)$	$158 \pm 3 (\pm 12)$	$1.39 \pm 0.02 (\pm 0.08)$		2.9
Power law times exponential with refl. @1.5	$0.473 \pm 0.001 (\pm 0.017)$	$156 \pm 3 (\pm 4)$	$0.96 \pm 0.04 (\pm 0.08)$		8.3

- (a) For the Thermal Bremsstrahlung and Sunyaev-Titarchuck model, the parameter is kT.  
For the exponentially truncated power law models, the parameter is the cutoff energy,  $E_c$ .

Table 3: Fits of an exponentially truncated power law  
to the individual Cyg X-1 observations.

Observation Number	Amp.@100 keV ( $\gamma \text{ cm}^{-2} \text{ s}^{-1} \text{ MeV}^{-1}$ ) $\times 10^{-3}$	$E_c$ (keV)	Photon Index	Luminosity <sup>(a)</sup> ( $\text{erg s}^{-1}$ ) $\times 10^{37}$
1	624±1	148±2	-1.22±.01	1.30
2	657±3	151±9	-1.21±.05	1.39
3	826±2	139±3	-1.18±.02	1.68
4	752±1	137±2	-1.28±.02	1.46
5	644±1	150±3	-1.34±.02	1.28
6	777±7	177±25	-1.55±.01	1.54
7	613±3	135±6	-1.14±.04	1.24
8	528±2	153±6	-1.29±.03	1.08
9	459±2	155±7	-1.70±.04	0.81
10	76±1	582±250	-2.52±.08	0.15
11	756±3	138±6	-1.30±.04	1.46
12	499±3	182±24	-1.79±.09	0.92
13	236±4	299±67	-2.16±.09	0.45
14	497±4	188±25	-1.64±.09	0.98
15	516±4	129±13	-1.43±.09	0.92
16	698±3	137±8	-1.16±.05	1.42
17	715±4	124±7	-1.01±.06	1.45

(a) Integral luminosity in the 60 keV-1MeV band.

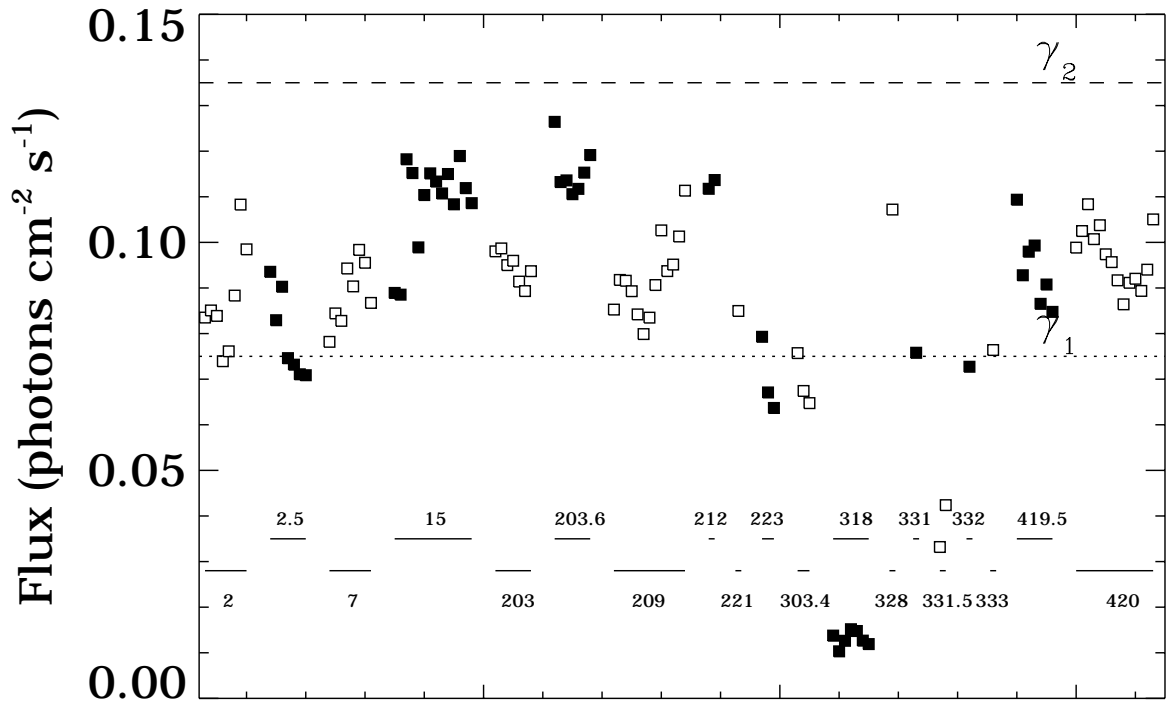


Figure 1: Flux in the 45-140 keV band for each day of Cyg X-1 data. The line segments show the viewing period associated with the data points. Also shown are the historic  $\gamma_1$  and  $\gamma_2$  states as defined by Ling et al. (1987). Alternate viewing periods are shown with open and filled squares.

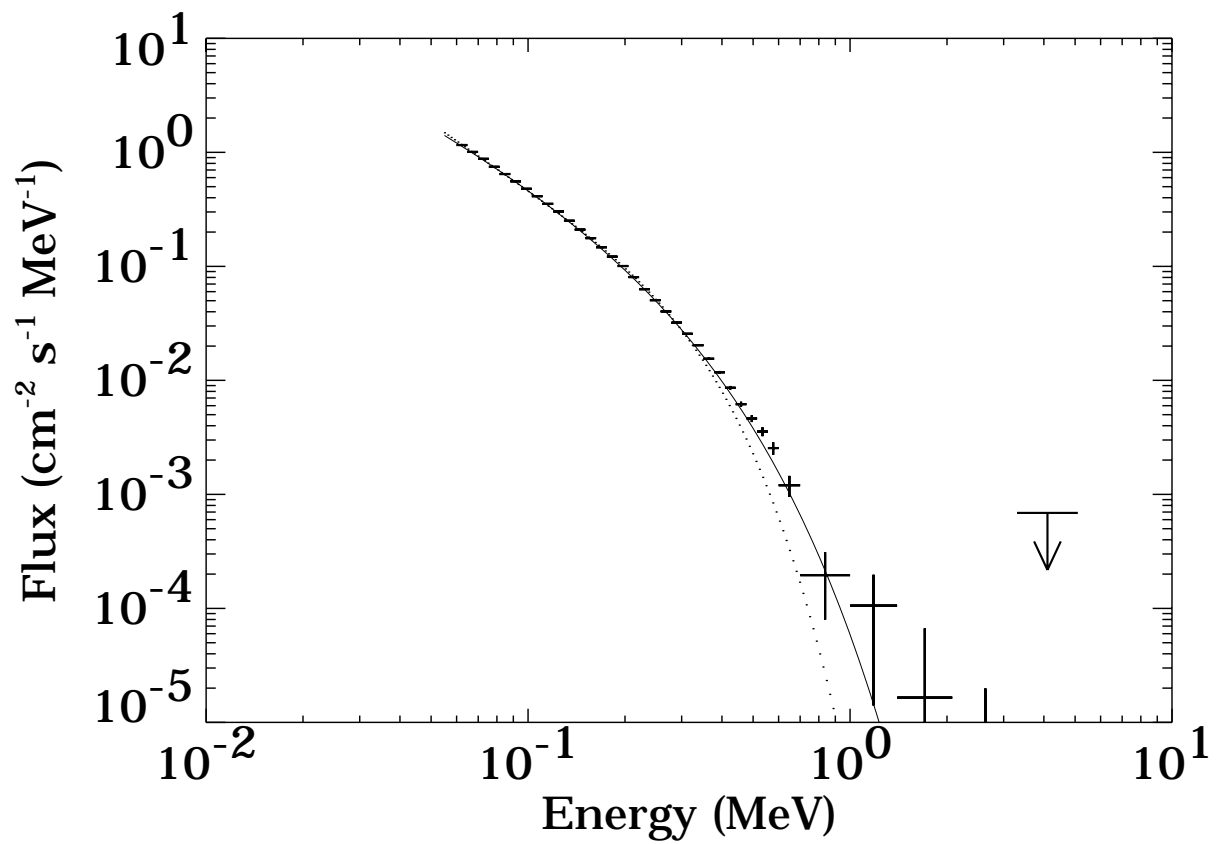


Figure 2: Spectrum of Cyg X-1 for all the data. The solid line is the best fit to the data with an exponentially truncated power law model while the dotted line is the best fit using the thermal Comptonization model of Sunyaev and Titarchuk (1980). Upper limits are 2 sigma. See Table 2 for the parameters of the fits.

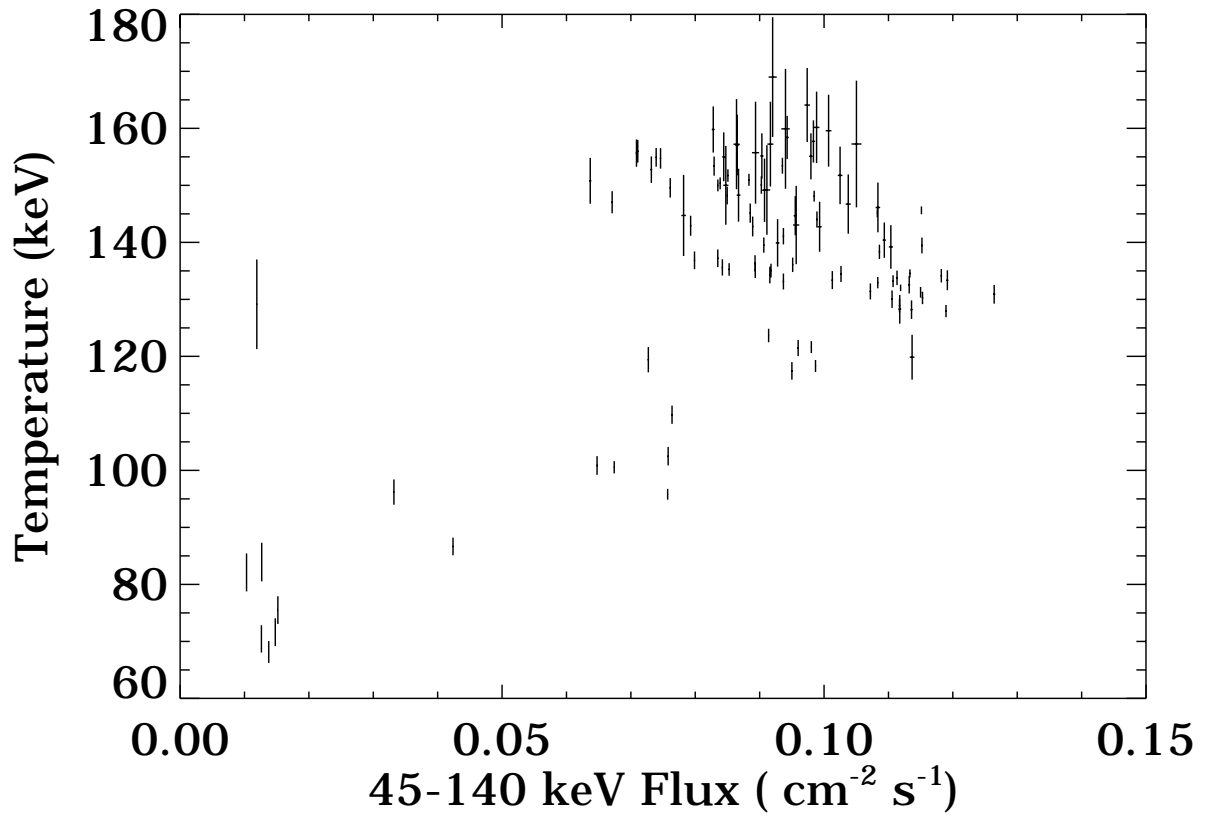


Figure 3: Temperature versus 45-140 keV integrated flux for each day obtained using an optically thin thermal bremsstrahlung model.

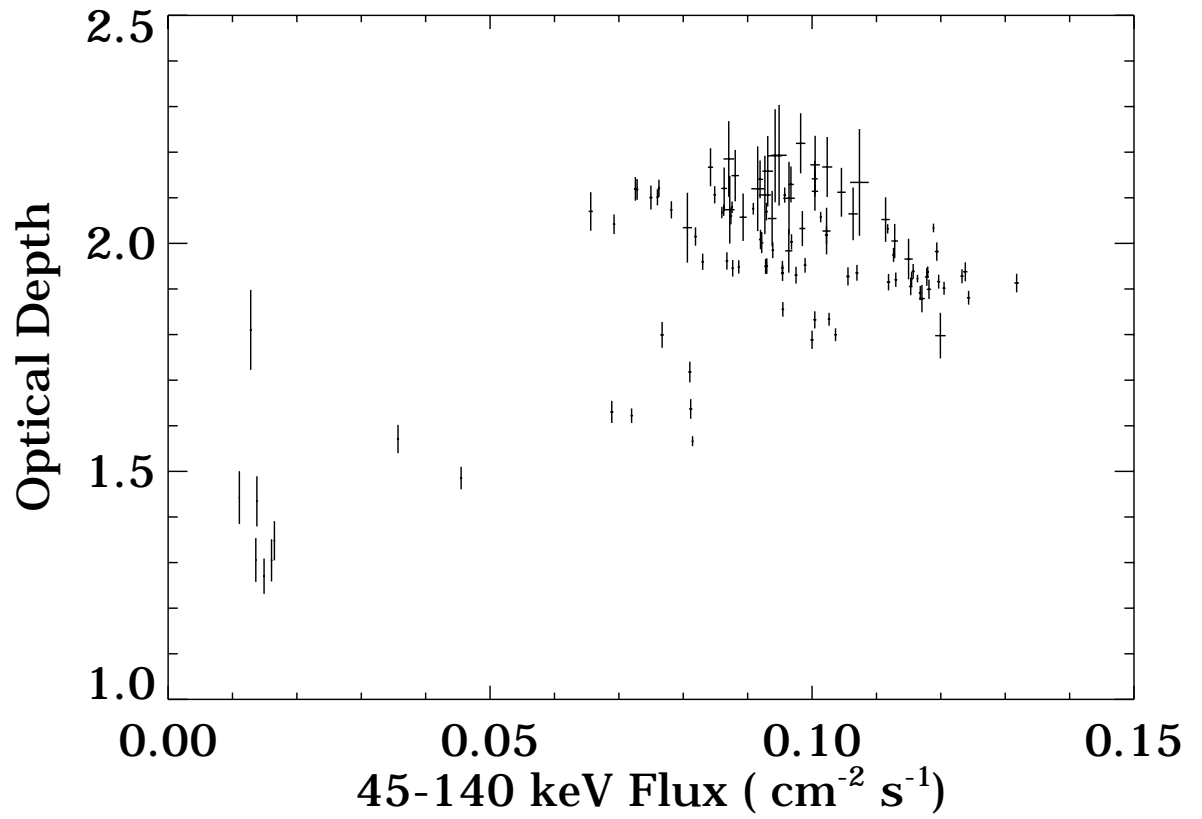


Figure 4: Optical depth versus 45-140 keV integrated flux for each day using the model of Sunyaev and Titarchuk (1980) with the temperature fixed at 65 keV.

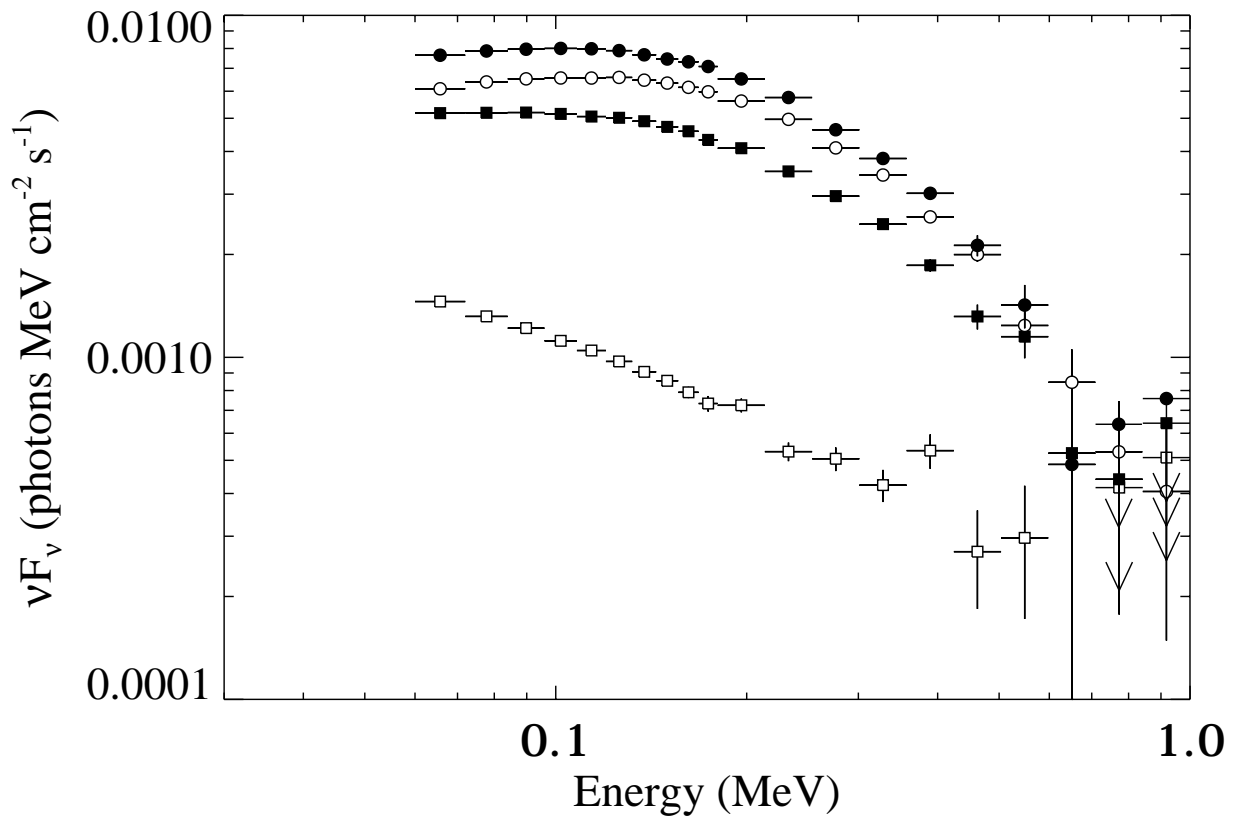


Figure 5: Photon spectrum multiplied by the energy squared. The data were grouped into four bins according to their 45-140-keV flux:  $<0.06$  photons  $\text{cm}^{-2} \text{s}^{-1}$ , between 0.06 and 0.08 photons  $\text{cm}^{-2} \text{s}^{-1}$ , between 0.08 and 0.105 photons  $\text{cm}^{-2} \text{s}^{-1}$ , and greater than 0.105 photons  $\text{cm}^{-2} \text{s}^{-1}$ .

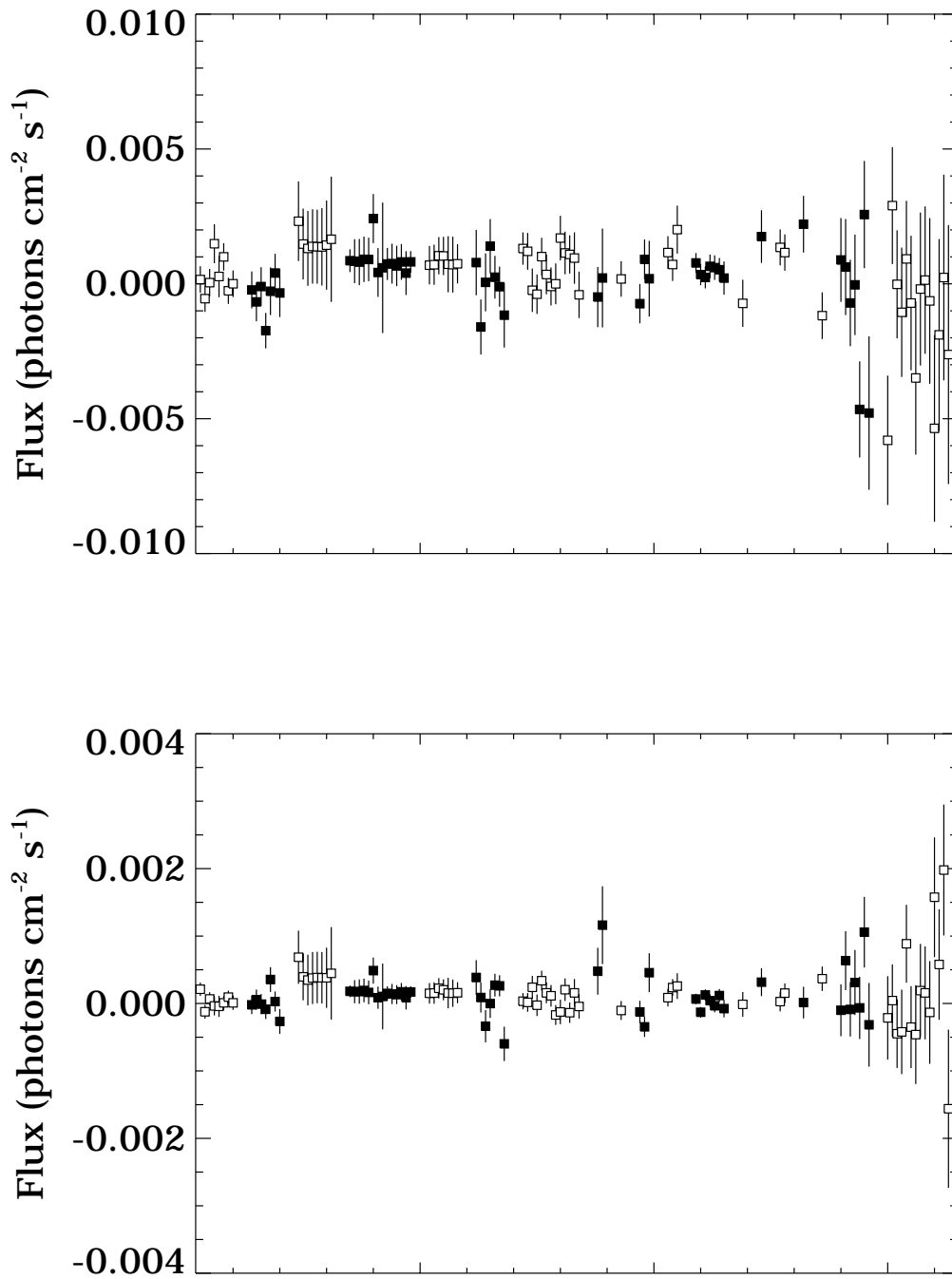


Figure 6: Amplitude and error of the 1 MeV gaussian fit (Figure 6a) and the narrow 511 keV line (Figure 6b) on top of a thermal bremsstrahlung continuum for each day of data. The X-axis is the same discontinuous time axis as in figure 1.

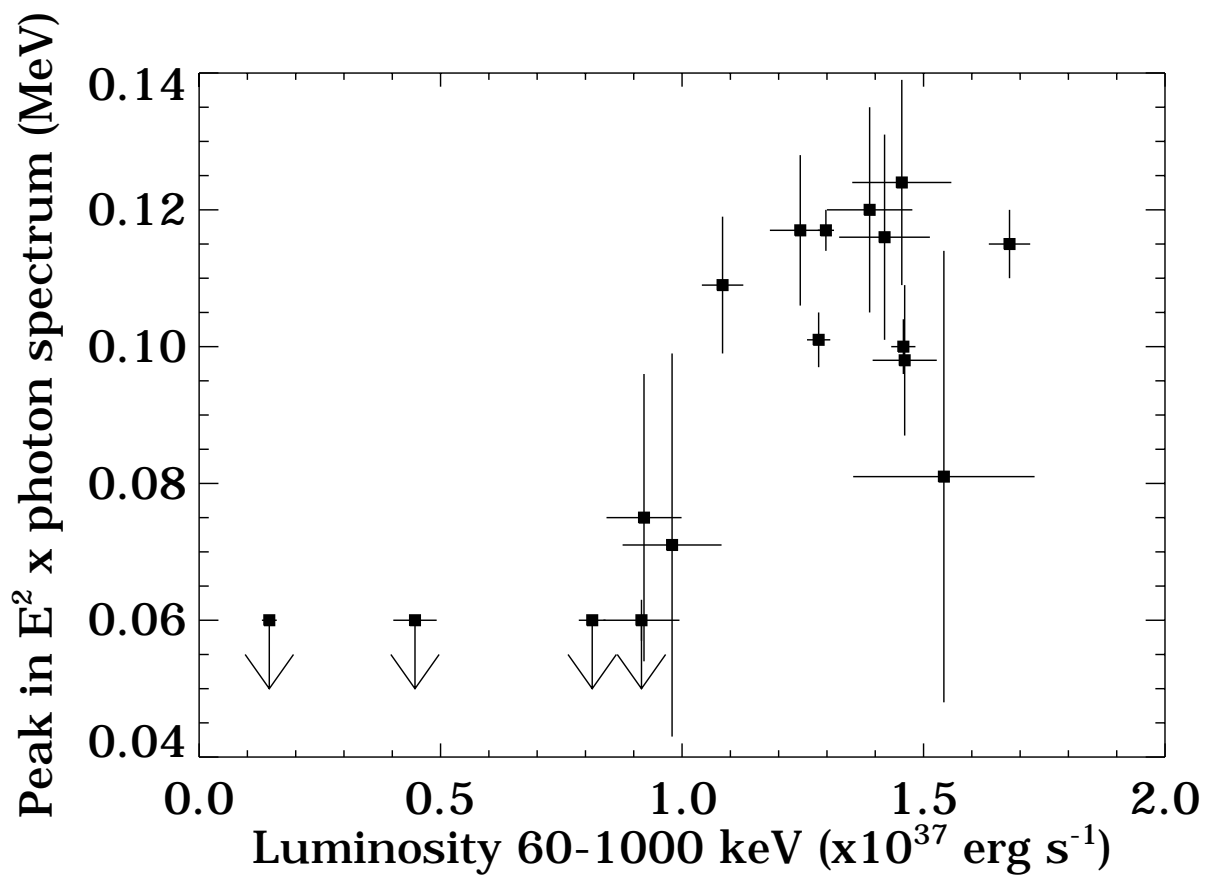


Figure 7: Peak in luminosity per decade versus luminosity between 60 and 1000 keV for the model fits of all the observations, as in Table 3.

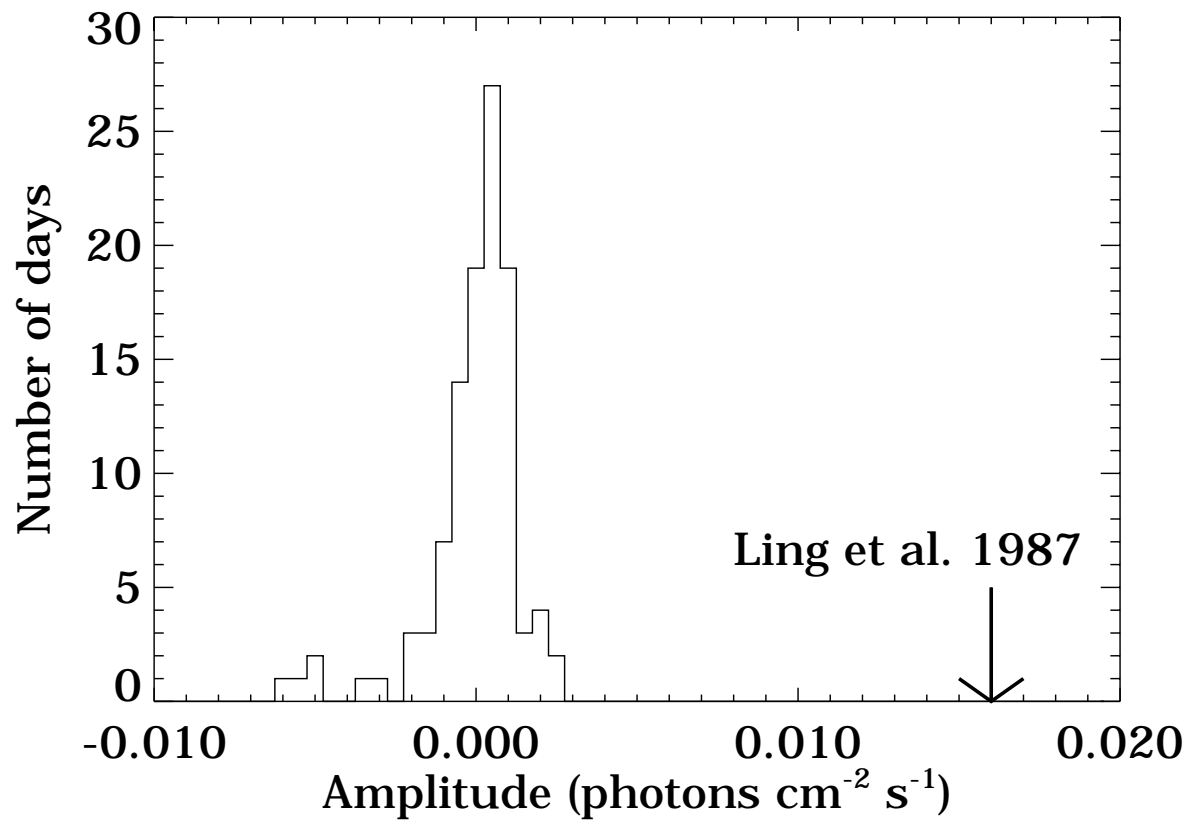


Figure 8: Distribution of the daily amplitudes of the 1 MeV gaussians. The amplitude reported by Ling et al. (1987) is shown for comparison.

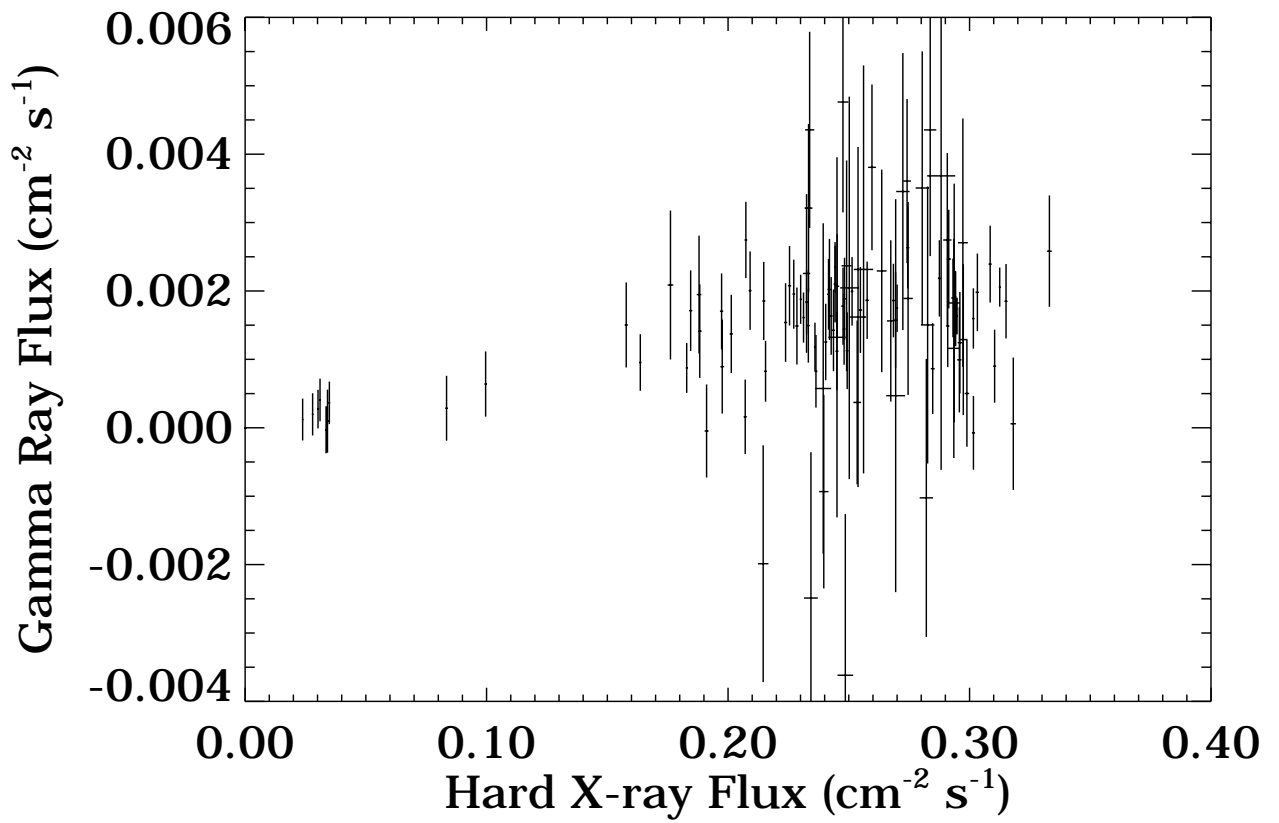


Figure 9: Flux in the 0.4-1.5 MeV band versus the flux in the 0.06-0.4 MeV band for each day of data. These bands are nearly identical to those in the compilation of Bassani et al. (1989).

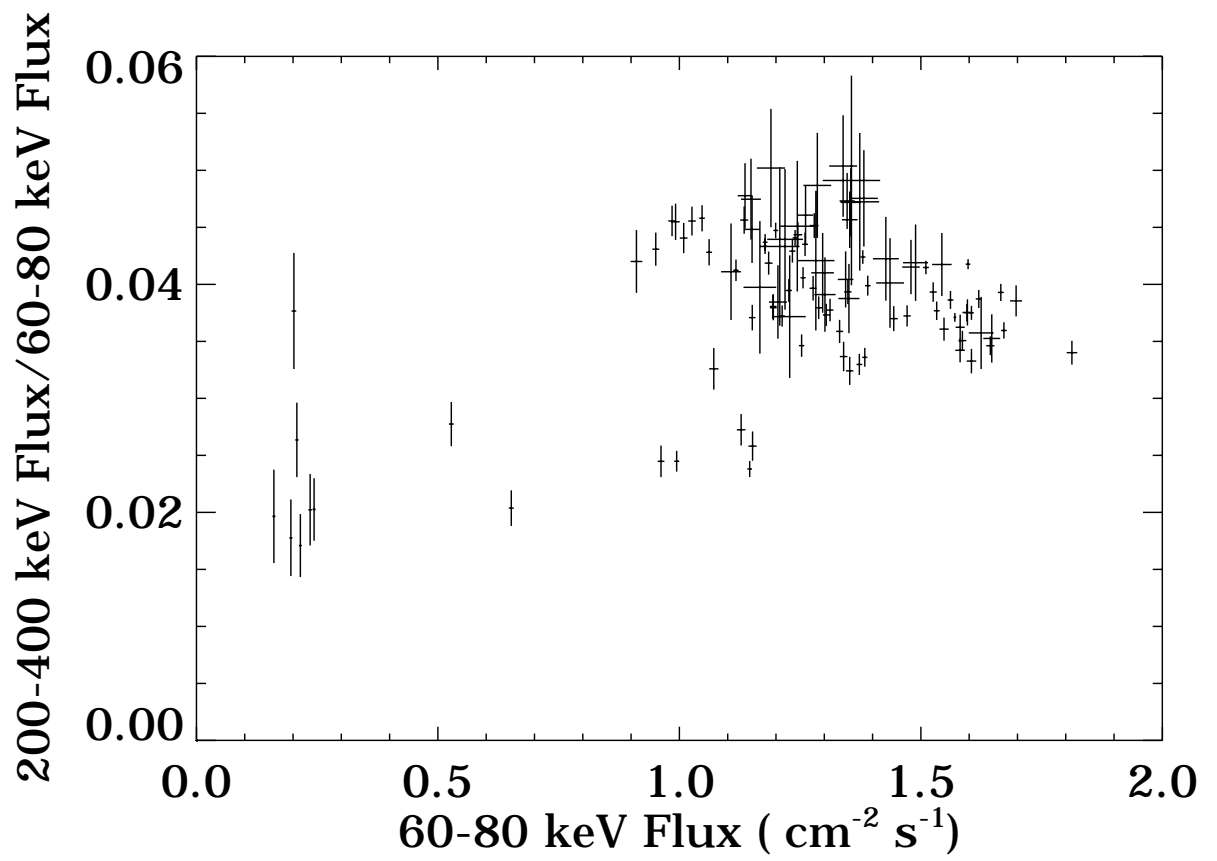


Figure 10: Ratio of the flux in the 200-400 keV band over the flux in the 60-80 keV band versus the flux in the 60-80 keV band for each day of data.